Geometry of the soluble methane monooxygenase catalytic diiron center in two oxidation states

Amy C Rosenzweig[1*], Pär Nordlund[2], Patricia M Takahara[3], Christin A Frederick[1] and Stephen J Lippard[3*]

[1]Department of Biological Chemistry and Molecular Pharmacology, Harvard Medical School, Dana Farber Cancer Institute, 44 Binney St., Boston, MA 02115, USA, [2]Department of Molecular Biology, University of Stockholm, S-10691 Stockholm, Sweden and [3]Department of Chemistry, Massachusetts Institute of Technology, Cambridge, MA 02139, USA

Background: The hydroxylase component of soluble methane monooxygenase (sMMO) contains a dinuclear iron center responsible for the oxidation of methane to methanol. As isolated, the center is in the oxidized, diiron(III) state. The 2.2 Å resolution X-ray structure of the oxidized hydroxylase, H_{ox}, from *Methylococcus capsulatus* (Bath) was previously determined at 4 °C. In this structure the two iron atoms are bridged by a glutamate, a hydroxide ion, and an acetate ion, and additionally coordinated to two His residues, three Glu residues, and a water molecule.
Results: The 1.7 Å resolution crystal structures of the sMMO hydroxylase from *Methylococcus capsulatus* (Bath) in both its oxidized diiron(III), H_{ox}, and dithionite-treated, reduced diiron(II), H_{red}, oxidation states were determined at −160 °C. The structure of the diiron center in H_{ox} differs from that previously reported at 2.2 Å resolution and 4 °C. Although the hydroxide bridge is retained, the bidentate, bridging ligand assigned as acetate is replaced by a weakly coordinating monoatomic water bridge. In the resulting four-membered $Fe(\overline{OH})Fe(\overline{OH_2})$ ring, the Fe···Fe distance is shortened from 3.4 Å to 3.1 Å. In protomer A of H_{red}, the hydroxide bridge is displaced by an oxygen atom of Glu243, which undergoes a carboxylate shift from its terminal monodentate binding mode in H_{ox} to a mode in which the carboxylate is both monoatomic bridging and bidentate chelating. We therefore conclude that the center has been reduced to the diiron(II) oxidation state. Both iron atoms are coordinated to five ligands and weakly to a sixth water molecule in the resulting structure. The diiron center in protomer B of H_{red} has the same composition as those in H_{ox}. In both the oxidized and reduced structures, the diiron core is connected through hydrogen bonds involving exogenous species to Thr213 in the active site cavity.
Conclusions: The diiron center in H_{ox} can change its exogenous ligand coordination and geometry, a property that could be important in the catalytic cycle of sMMO. In H_{red}, a carboxylate shift occurs, extruding hydroxide ion and opening coordination sites for reaction with O_2 to form the diiron(III) peroxo intermediate, H_{peroxo}. Residue Thr213 may function in catalysis.

Chemistry & Biology June 1995, **2**:409–418

Key words: carboxylate shift, dinuclear iron center, methane oxidation, *Methylococcus capsulatus* (Bath), X-ray crystallography

Introduction

Methane oxidation (equation 1) by the soluble methane monooxygenase (sMMO) enzyme systems from methanotrophic bacteria occurs at a catalytic dinuclear iron center located on the α subunit of the multisubunit ($\alpha_2\beta_2\gamma_2$) hydroxylase protein [1–3].

$$CH_4 + NADH + H^+ + O_2 \rightarrow CH_3OH + NAD^+ + H_2O \quad \textbf{(Equation 1)}$$

In the resting state of the isolated hydroxylase protein, the diiron center is in the diferric, Fe(III)Fe(III), oxidation level (H_{ox}). During the catalytic cycle, the center is reduced to the diferrous, Fe(II)Fe(II), state (H_{red}) by two electrons which are transferred to the hydroxylase from NADH through the reductase (R, 38.6 kDa), an iron–sulfur flavoprotein. The electron transfer is regulated by a third component, protein B (15.5 kDa), that has no cofactors. H_{red} then reacts with dioxygen in the presence of protein B to form two intermediates sequentially. These have been studied by stopped-flow optical ([4] and K.E. Liu, A.M. Valentine, D. Wang, B.H. Huynh, D.E. Edmondson, A., Salifoglou & S.J.L., unpublished data), freeze-quench Mössbauer [5,6], and resonance Raman [7] spectroscopy. The first intermediate, H_{peroxo}, forms with a rate constant of ~25 s^{-1} and exhibits an isotope-sensitive feature in the resonance Raman spectrum at 905 cm^{-1}, which has been assigned as the O–O stretching frequency of a diiron(III) peroxo unit [7]. It has been suggested that the peroxo ligand coordinates to the iron atoms in either the μ-η^1:η^1 or nonplanar μ-η^2:η^2 binding modes ([6,8] and K.E. Liu *et al.*, unpublished data). H_{peroxo} is then converted to a second intermediate, Q, which forms with a rate constant of 0.5–1.0 s^{-1}, depending on the organism ([4–6] and K.E. Liu *et al.*, unpublished data). Intermediate Q has optical features with λ_{max} ~350 and ~420 nm and unusual Mössbauer parameters. In the final steps of the reaction cycle, Q reacts with substrate to form product and regenerate H_{ox}. The structure of Q and the mechanism by which it hydroxylates substrate are presently unknown, but several possibilities have been discussed elsewhere [1,3–6,8].

Detailed structural information about the diiron center is essential to a complete understanding of the catalytic

*Corresponding authors.

 ISSN 1074-5521

mechanism. Previously we reported the 2.2 Å resolution 4 °C X-ray structure determination of H_{ox} from *M. capsulatus* (Bath) [9]. We have now extended the resolution limit of the hydroxylase crystals to better than 1.7 Å by employing cryo-crystallographic methods. This high resolution study has enabled us to provide better metrical details of the active site structure. Here we present the geometry of the diiron center in both the oxidized and chemically reduced forms as revealed by the 1.7 Å resolution crystal structures. In H_{red}, one of the glutamate ligands adopts an altered coordination mode which, although known in diiron model compounds, is unprecedented in biological diiron centers. In the high resolution, frozen crystal structure of H_{ox}, the geometry of the dinuclear iron center changes from that previously found in the 2.2 Å resolution, 4 °C determination, through a switch in the coordination modes of the exogenous ligands with an attendant reduction in Fe···Fe distance. These findings have important implications both for our understanding of the hydroxylation mechanism and for the preparation of replicative models.

Results

Structure of H_{ox}

The structure of the dinuclear iron center in H_{ox} as revealed by the 1.7 Å crystal structure determination is shown in Figure 1. Metrical details of the coordination geometry are presented in Table 1. Most features of the diiron center are identical to what was previously observed in the 2.2 Å resolution, 4 °C structure analysis [9]. Each iron atom is coordinated to the δ-nitrogen atom of a histidine residue, His147 or His246, with Fe–N distances of ~2.1 Å. There is one semi-bridging glutamic acid residue, Glu144, as in the 2.2 Å structure, with normal coordinating distances for Fe1–O and longer distances for Fe2–O (Table 1). Fe1 is coordinated to one monodentate carboxylate ligand, Glu114, and Fe2 is ligated by two such monodentate carboxylates, Glu209 and Glu243. Fe1 is also bonded to a terminal water molecule, which is hydrogen bonded to the uncoordinated or 'dangling' oxygen atoms of both Glu114 and Glu243 (Fig.1 and Table 1). A Fourier map at the diiron center in H_{ox} is shown in Figure 2. The electron density for Glu243 is not as well defined as that for the other carboxylate residues, suggesting that it may be somewhat disordered. In particular, the uncoordinated oxygen atom OE2 has a high B-value of ~30 $Å^2$ and may occupy more than one position, the average of which is within hydrogen bonding distance of the terminal water molecule.

Two exogenous bridging ligands, revealed in difference Fourier electron density maps, also link the two iron atoms. In Figure 2, the difference density for these ligands and for the terminal water bound to Fe1 is superimposed on the final $2F_o–F_c$ map. One of the exogenous bridging ligands, assigned as hydroxide rather than oxo in accord with the spectroscopic properties of the oxidized and mixed valent *M. capsulatus*

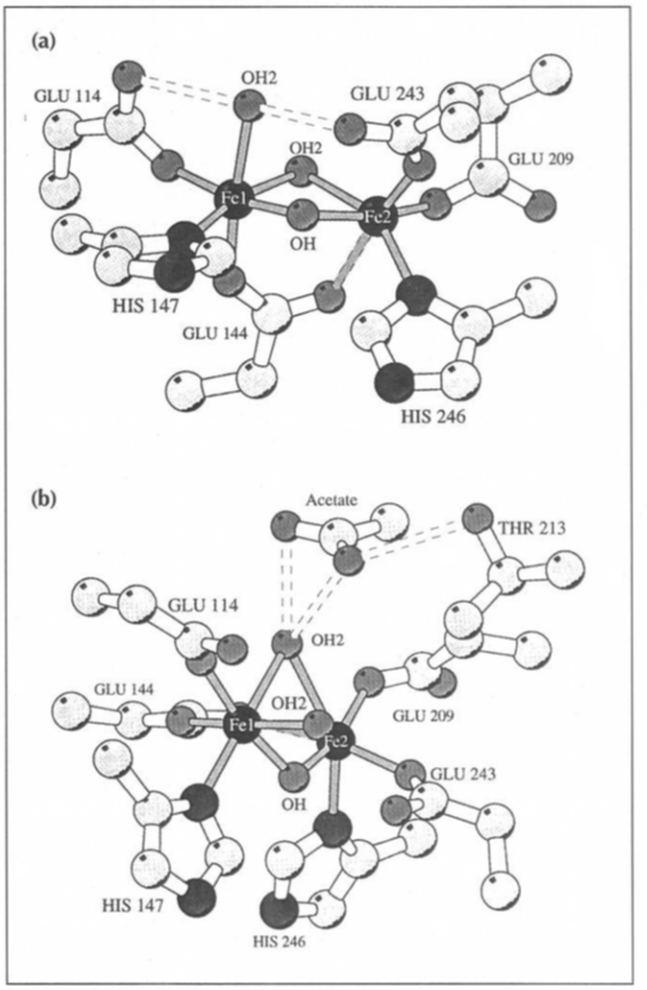

Fig. 1. Structure of the dinuclear iron center in H_{ox}. **(a)** Overall view. Open dashed lines indicate hydrogen bonds. The filled dashed line indicates a weak interaction. **(b)** Expanded view of the center showing an exogenous acetate ion in the active site cavity and threonine residue Thr213. The acetate ion is hydrogen-bonded both to the water bridge and to Thr213. Hydrogen bonds involving the terminal water molecule are omitted.

(Bath) hydroxylases [10,11], was also present in the 2.2 Å resolution structure. Although the Fe1–μOH distance is ~0.3 Å shorter than the Fe2–μOH bond lengths in both protomers (Table 1), the observed bond length asymmetry is not outside experimental error. The second exogenous bridge, however, differs from what was observed in the 2.2 Å structure. Instead of electron density ascribed to a bidentate, bridging acetate ion from the crystallization buffer, the 1.7 Å resolution structure reveals a monoatomic bridge, which we assign as a weakly coordinated water molecule. The average Fe–O distances for this bridging ligand of 2.5 Å in the A protomer and 2.4 Å in the B protomer are consistent with such an assignment. Each Fe atom is therefore six-coordinate, the geometry of both Fe atoms being approximately octahedral. Accompanying this change in exogenous bridging ligand is a reduction in the Fe···Fe distance from 3.4 Å to 3.1 Å. This result is obtained in both halves of the dimer, the Fe···Fe

Table 1. Interatomic distances (Å)[a] in H_{ox}[b].

Atom	Atom	Distance (Å)		
		Protomer A	Protomer B	Average
Fe1	Fe2	3.04	3.14	3.1
Fe1	Glu114 OE1	1.91	1.96	1.9
Fe1	His147 ND1	2.13	2.15	2.1
Fe1	Glu144 OE2	2.00	2.19	2.1
Fe1	μOH	1.78	1.62	1.7
Fe1	OH_2	2.28	2.27	2.3
Fe1	μOH_2	2.43	2.24	2.3
Fe2	Glu209 OE2	1.96	1.85	1.9
Fe2	His246 ND1	2.32	2.08	2.2
Fe2	Glu243 OE1	1.95	2.04	2.0
Fe2	Glu144 OE1	2.44	2.56	2.5
Fe2	μOH	1.94	2.02	2.0
Fe2	μOH_2	2.58	2.51	2.5
OH_2	Glu114 OE2	2.92	2.65	2.8
OH_2	Glu243 OE1	2.74	3.16	3.0
OH_2	μOH	2.58	2.76	2.7
μOH_2	Ac O1	2.62	2.63	2.6
μOH_2	Ac O2	2.97	2.84	2.9
Ac O2	Thr213 OG1	3.11	2.91	3.0

[a]Estimated standard deviations in distances are ~0.2 Å.
[b]Protomers A and B are the two crystallographically independent halves of the hydroxylase $\alpha_2\beta_2\gamma_2$ dimer (see [9]).

distances being 3.14 Å in the A protomer and 3.04 Å in the B protomer. In addition, the Fe1–μOH–Fe2 bond angle is reduced from 133° and 131° to 109° and 120° for the A and B protomers, respectively.

The electron density previously assigned as an acetate ion in the 4 °C, 2.2 Å structure has not completely disappeared, however. The Fourier maps revealed residual density in the active site cavity, within hydrogen bonding distance of the bridging water molecule, but not coordinated to the iron atoms. This density is significantly larger than expected for a water molecule. We therefore continue to assign it as an acetate ion, although other possibilities exist [9], since 50 mM NH_4OAc was present in the crystallization buffers. The electron density is not extremely well defined, however, suggesting possible disorder. The two oxygen atoms of the proposed acetate ion are within hydrogen bonding distance of the bridging water ligand and OG1 oxygen atom of Thr213 (Fig. 1b, Table 1), supporting the assignment of the extra electron density as a carboxylate species. The presence of this acetate ion retains the overall charge neutrality of the active site.

Structure of H_{red}

The structure of the chemically reduced hydroxylase protein is very similar to that of H_{ox} [9], except at the diiron center in one of the two halves of the $\alpha_2\beta_2\gamma_2$ dimer. In particular, the coordination of the diiron center within the A protomer differs significantly from that in H_{ox}, whereas the B protomer more closely resembles the oxidized hydroxylase. This result strongly suggests that, in the crystal, a change in oxidation state resulting from the addition of dithionite and methyl viologen occurs at the diiron center of the A protomer. The structure of this center is shown in Figure 3, and metrical information about both centers is provided in Table 2. Before presenting the differences, we note that the chemically reduced diiron center in protomer A of H_{red} has many features in common with those in H_{ox} and in protomer B of H_{red}. Each iron atom is coordinated to the δ-N atom of a histidine ligand, and Glu144 remains semi-bridging. In addition, Fe1 and Fe2 are each coordinated to one monodentate, terminal glutamic acid residue, Fe1 to Glu114 and Fe2 to Glu209. Despite these similarities, the coordination mode of Glu243 has changed dramatically in protomer A of H_{red} (Fig. 3). In H_{ox} and protomer B of H_{red}, Glu243 binds to Fe2 in a monodentate, terminal mode. In protomer A of H_{red}, however, this residue has become a bidentate, chelating ligand to Fe2 as well as a monodentate bridging ligand. Although the Fourier map (Fig. 4) reveals that, as in H_{ox}, the electron density is not as well defined for this residue as for the other glutamates, the similar thermal parameters for the two oxygen atoms, ~19 $Å^2$ for OE1 and ~17 $Å^2$ for OE2, are consistent with both being coordinated to iron, and the average position for OE2 is clearly different from that in H_{ox}. In particular, this oxygen atom, which was not coordinated in the oxidized structure, now clearly bridges the two iron atoms, the average Fe–OE2 distance being 2.2 Å. The distance for the nonbridging, coordinated oxygen atom, Fe2–OE1, is 2.3 Å, and the Fe···Fe separation is 3.28 Å.

Of the three exogenous ligands found in H_{ox}, two persist in protomer A of H_{red}, the terminal water molecule coordinated to Fe1, $OH_2(2)$, and the bridging water, $OH_2(1)$, now bound only very weakly to Fe2. No electron density for the bridging hydroxide was present in difference Fourier maps. The Fourier maps for the diiron(II) center are shown in Figure 4. Since it is known from spectroscopic studies that the oxidized Fe(III)Fe(III) and mixed valent Fe(II)Fe(III) hydroxylases both contain

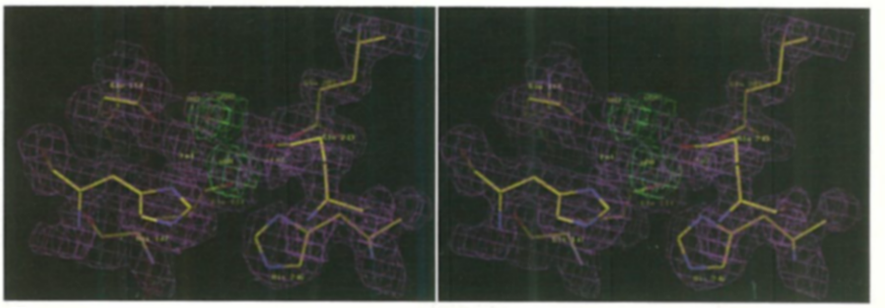

Fig. 2. Stereo representation of the final $2F_o–F_c$ electron density at the diiron center in H_{ox}. The $2F_o–F_c$ map is shown in blue and is contoured at the root-mean square (rms) density. The $F_o–F_c$ difference electron density map, showing the hydroxo and water bridges and the water molecule coordinated to Fe1, is superimposed in green, and is contoured at three times the rms density.

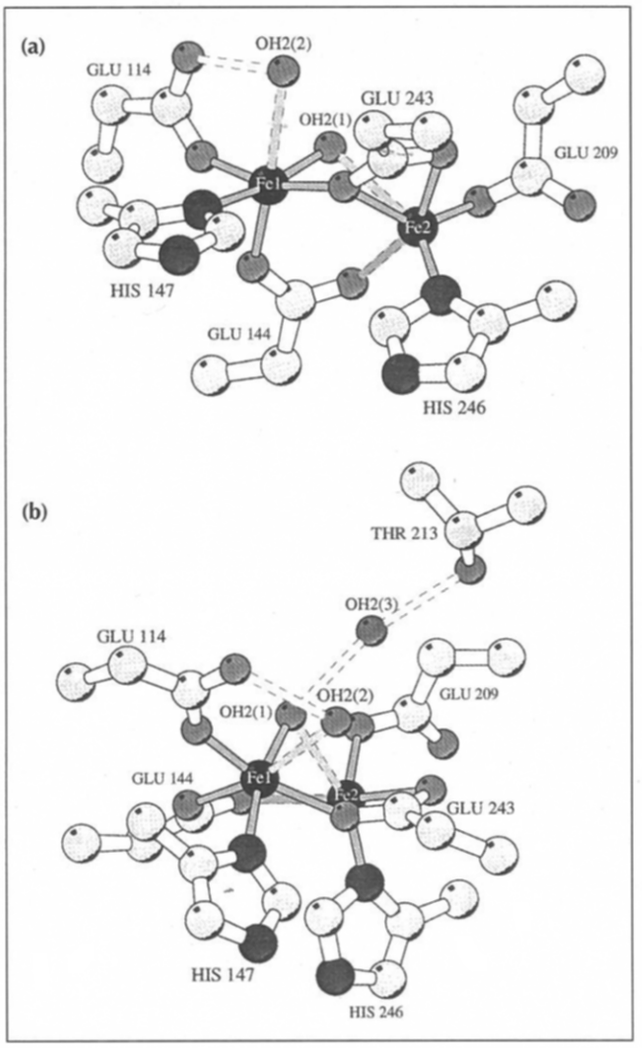

Fig. 3. Structure of the dinuclear iron center in H_{red}. **(a)** Overall view. Open dashed lines indicate hydrogen bonds. Filled dashed lines indicate weak interactions. The long Fe1–OH_2(2) and Fe2–OH_2(1) distances (Table 1) suggest little bonding interaction. **(b)** Expanded view of the center showing a third water molecule in the active site cavity and threonine residue Thr213. This water molecule, labeled OH2(3), is hydrogen bonded both to the water bridge and to Thr213.

a hydroxo bridge [10,11], we assign the species obtained in protomer A of H_{red} to the fully reduced diiron(II) state. Although OH_2(2) occupies the same position as the terminal water ligand in the oxidized structure, the Fe1–O distance is long, 2.6 Å. This water molecule is therefore very weakly bound. The second water molecule, OH_2(1), is situated in the space where the bridging water molecule is located in the oxidized structure, but coordinated mainly to Fe1. The distances are Fe1–O, 1.9 Å, a value within error of that expected from model chemistry [12] and Fe2–O, 2.7 Å. We therefore consider both iron atoms at the reduced center to be essentially five-coordinate, each having a weakly interacting water ligand interaction at the sixth, octahedral site. The geometry at Fe2 is more distorted owing to the bidentate coordination mode of Glu243. The active site cavity in protomer A of H_{red} also contains a third water molecule, evident in the difference Fourier map, in the position that is occupied by an acetate ion in H_{ox} (Fig. 1b). This water molecule, labeled OH_2(3), is hydrogen bonded to OH_2(1), thereby linking OH_2(1) and Thr213 (Fig. 3b).

The diiron center in protomer B of the chemically reduced hydroxylase is similar to the oxidized centers in H_{ox} with respect to ligand composition and coordination number. All three exogenous ligands, the terminal water molecule on Fe1, the bridging hydroxide, and the bridging water molecule, appeared in difference Fourier maps. In addition, Glu243 remains a terminal, monodentate ligand to Fe2. A poorly defined portion of electron density is also present in the position occupied by the acetate ion in H_{ox}. There is one metrical difference between the diiron center in protomer B of the chemically reduced hydroxylase and the oxidized hydroxylase, however (Tables 1 and 2), which appears to be outside experimental error. The Fe···Fe distance is 3.43 Å, instead of ~3.1 Å. This increase is accompanied by a lengthening of the Fe1–O distance for the bridging water molecule from 2.5 Å to 2.7 Å.

Discussion

The catalytic center of H_{red}

The molecular architecture of the catalytic center in H_{red} is of great interest since it is this form of the enzyme that reacts with dioxygen. As indicated in Figures 1 and 3, the diiron center in protomer A of H_{red}

Table 2. Interatomic distances (Å)[a] in H_{red}[b].

Atom	Atom	Distance (Å)	
		Protomer A[c]	Protomer B[d]
Fe1	Fe2	3.28	3.43
Fe1	Glu114 OE1	1.90	1.93
Fe1	His147 ND1	2.39	2.31
Fe1	Glu144 OE2	2.15	2.00
Fe1	μOH	N/A	1.56
Fe1	OH_2(1)[e]	1.92	2.08
Fe1	OH_2(2)	2.63	N/A
Fe1	μOH_2	N/A	2.67
Fe1	Glu243 OE2	2.10	N/A
Fe2	Glu209 OE2	2.27	1.86
Fe2	His246 ND1	1.94	2.07
Fe2	Glu243 OE2	2.33	1.97
Fe2	Glu243 OE1	2.33	N/A
Fe2	Glu144 OE1	2.39	2.26
Fe2	μOH	N/A	2.23
Fe2	μOH_2	N/A	2.52
Fe2	OH_2(1)	2.72	N/A
OH_2(1)[e]	Glu114 OE2	3.59	2.61
OH_2(2)	Glu114 OE2	2.60	N/A
OH_2(1)	OH_2(3)	2.62	N/A
OH_2(3)	Thr213 OG1	2.73	N/A

[a]Estimated standard deviations in distances are ~0.25 Å.
[b]Protomers A and B are the two crystallographically independent halves of the hydroxylase $\alpha_2\beta_2\gamma_2$ dimer (see [9]).
[c]Chemically reduced diiron center.
[d]Oxidized or partially reduced diiron center.
[e]For the B protomer, the water molecule labeled OH_2(1) corresponds to the water molecule labeled OH_2 in Table 1.

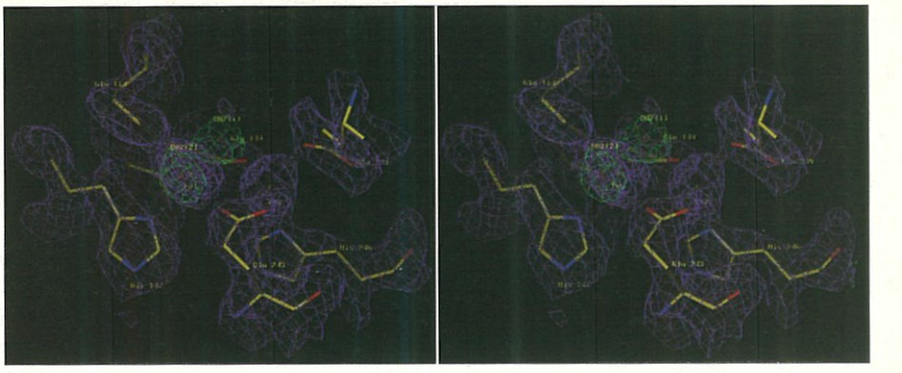

Fig. 4. Stereo representation of the final $2F_o$-F_c electron density at the diiron center in H_{red}. The $2F_o$–F_c map is shown in blue and is contoured at the rms density. The F_o–F_c difference electron density map, showing the two water molecules coordinated to Fe1, is superimposed in green, and is contoured at three times the rms density.

differs significantly from that in H_{ox} and in protomer B of H_{red}. The hydroxide bridge has been displaced by an oxygen atom of Glu243, which adopts an altered coordination mode. For the reasons indicated above, we conclude that the dinuclear iron center in protomer A has been reduced to the diiron(II) state. The similarity of the diiron center in protomer B to that in crystals not treated with chemical reductants suggests that it remains at least partially oxidized. We considered the possibility that a fraction of the diiron centers in protomer B may have been reduced to the diiron(II) state, leading to a superposition of structures, which could account for the longer Fe···Fe distance. The thermal parameters of the Fe atoms in protomer B of H_{red} are very similar to those in protomer A and the two centers in H_{ox}, however. In each case, the B-values range from ~9–14 Å^2 for Fe1 and from ~19–22 Å^2 for Fe2. This similarity makes it seem less likely that the B protomer of H_{red} crystals contains a mixture of oxidation states. Another possibility is that the diiron center in protomer B has been partially reduced to the mixed valent, Fe(II)Fe(III) state. The hydroxo bridge and terminal water ligand are retained in this state as demonstrated by ENDOR spectroscopic studies [10], and the Fe···Fe distance is known from EXAFS to be 3.4 Å [11].

The geometries of the diiron(II) and diiron(III) centers are superimposed in Figure 5. The structure of the reduced center agrees reasonably well with the interpretation of a magnetic circular dichroism (MCD) study of *M. trichosporium* OB3b H_{red}, from which it was concluded that two five-coordinate Fe atoms were present having different geometries [13]. The coordination geometries of the two Fe(II) atoms in the present structure determination clearly differ from one another, with Fe2 being much more distorted. Although there are six ligands at octahedral sites around each iron atom, only five are at distances corresponding to normal metal–ligand bonds. In the MCD study of the *M. trichsoporium* OB3b hydroxylase, the two ferrous atoms were ferromagnetically coupled with a J value of 0.3–0.5 cm^{-1}, where $\mathcal{H} = -2J\,\mathbf{S_1}\cdot\mathbf{S_2}$, and the presence of a water bridge was postulated. We do not see a normal water bridge in the *M. capsulatus* (Bath) hydroxylase diiron(II) center, only terminal water ligands on Fe1, one of which is weakly associated with Fe2. On the other hand, the bridging oxygen atom of Glu243 can probably serve as well as a bridging water ligand to mediate the magnetic exchange interaction [14]. Since differences in the reaction chemistry of the hydroxylases from the two organisms have been observed [3], however, we cannot rule out the possibility that H_{red} from *M. trichosporium* OB3b may contain a water bridge. Nevertheless, the present H_{red} structure is fully consistent with all available data for H_{red} from both organisms, including the sign of the exchange coupling constant [13,14].

The change in Glu243 coordination mode is a significant difference between the H_{red} and H_{ox} structures. Such an alteration of carboxylate coordination in a dimetallic center is not unprecedented, and illustrates a phenomenon known as the 'carboxylate shift' [15]. Carboxylate shifts describe structural variations in the binding of RCO_2^- fragments to polymetallic centers which were first observed for several crystallographically characterized model compounds and postulated to occur in metalloproteins. From an analysis of compounds having monodentate bridging carboxylate ligands, it was possible to classify them according to the degree of interaction between the nonbridging, or 'dangling', oxygen atom

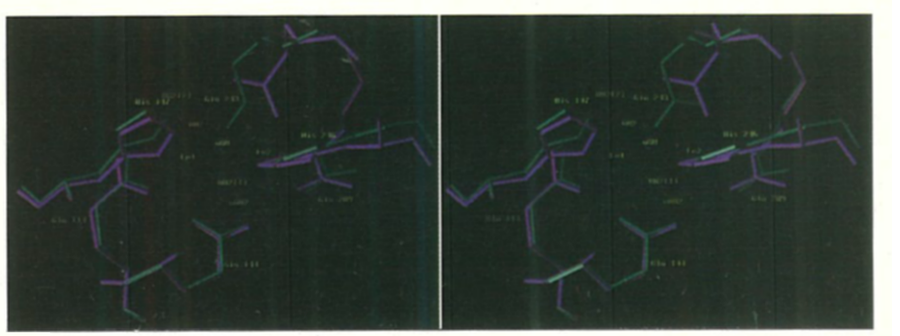

Fig. 5. Stereo superposition of the dinuclear iron centers in H_{ox} and H_{red}. H_{ox} is shown in purple and H_{red} in light blue.

and one of the bridged metal atoms [15]. One such diiron(II) compound, $[Fe_2(O_2CH)_4(BIPhMe)_2]$ [16], contains a monodentate bridging formate which becomes a monodentate terminal ligand upon oxidation to the diiron(III) state (Fig. 6a). This chemistry is very similar to what happens in H_{red}, although the dangling oxygen atom of the formate in the diiron(II) complex is not coordinated to Fe2, the Fe–O distance being 2.79 Å. The Glu243 carboxylate binding mode in H_{red} has previously been encountered in proteins, specifically, at the Mn(II)Ca(II) dimetallic center of concanavalin A [17].

A carboxylate shift also occurs upon oxidation of the R2 protein of ribonucleotide reductase. In this protein, reaction of dioxygen with the diiron(II) center generates a tyrosyl radical essential for enzyme activity [18,19], and both the diiron(II) and diiron(III) forms have been crystallographically characterized [20–22]. In the reduced R2 protein, Glu238 bridges the two Fe atoms (Fig. 6b) [21], but unlike Glu243 in H_{red}, this carboxylate ligand is bidentate, rather than monodentate, and does not form a chelate to Fe2. Consequently, the Fe···Fe distance of 3.8 Å in reduced R2 is significantly longer than the 3.28 Å Fe···Fe distance in H_{red}. Moreover, the reduced R2 protein contains no exogenous ligands in the vicinity of the two Fe atoms, which are therefore four-coordinate instead of five-coordinate as in H_{red}. Upon oxidation to the diiron(III) form, Glu238 becomes a monodentate terminal ligand, similar to Glu243 in H_{ox}.

The distinctive geometries of the reduced hydroxylase and R2 protein reveal how carboxylate shifts can alter the coordination sphere of diiron centers in what are otherwise very similar protein domains [9]. In the complete sMMO system, the hydroxylase is reduced to the diiron(II) state by R in the presence of protein B, a transformation we have effected chemically in the crystals. When all three sMMO components are present, interactions between proteins in the complex might facilitate reduction of H_{ox} by promoting the carboxylate shift of Glu243. This possibility is supported by the observation that, in the presence of substrate, protein B, and R, the reduction potential of H_{ox} becomes considerably more positive [23]. Thus the carboxylate shift, and concomitant hydroxide ion extrusion and weakening of two Fe–O(water) bonds, could provide the thermodynamic driving force to raise the reduction potential in a manner analogous to the alteration of the potential in cytochrome P-450 by thiolate binding and a spin state change [24]. The values of the reduction potentials of mononuclear Fe(III) model compounds become more positive with more nitrogen and fewer oxygen donor ligands [25]. In the complete sMMO system, therefore, protein B binding may facilitate loss of oxygen donor ligands, like the hydroxo and water bridges, raising the N:O ratios and increasing the reduction potentials. Direct evidence that protein B alters the coordination of the diiron center comes from its ability to affect the EPR and MCD spectra of the hydroxylase [13,26].

In the MCD study of the *M. trichosporium* OB3b hydroxylase [13], protein B appeared to perturb only one of the Fe atoms. As reported previously [9], two of the iron-binding helices, E and F, of H_{ox} from *M. capsulatus* (Bath) lie exposed on the walls of a canyon at the center of the protein, where protein B was postulated to

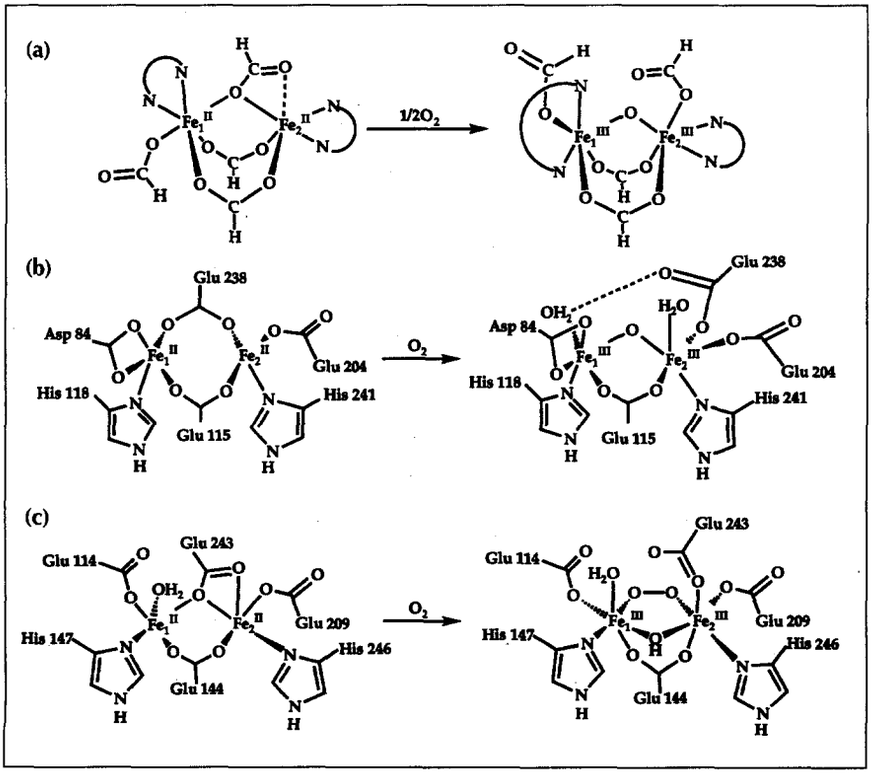

Fig. 6. Reactions of diiron(II) centers with dioxygen. **(a)** Reaction of $[Fe(O_2CH)_4(BIPhMe)_2]$ with dioxygen [16]. Note the carboxylate shift of one of the formate ligands. The ligand BIPhMe, bis(1-methylimidazol-2-yl)phenylmethoxymethane, is represented by $\widehat{N\ N}$. **(b)** Reaction of the reduced, diiron(II) ribonucleotide reductase R2 protein. Glutamic acid residue Glu238 changes from a bidentate, bridging ligand to a monodentate, terminal ligand upon oxidation. **(c)** Postulated structural changes accompanying the conversion of H_{red} to H_{peroxo} in the reaction with dioxygen. The carboxylate shift is analogous to that occurring between H_{ox} and H_{red}. Although the peroxide bridge is drawn in the μ-η^1:η^1 binding mode, several other possibilities exist as delineated elsewhere ([3] and K.E. Liu *et al.*, unpublished data). Weakly coordinating water interactions are not shown (compare Fig. 3a).

bind [9]. These two helices provide the iron-coordinating residues His246, Glu243, and Glu209, all of which coordinate to Fe2. We therefore propose that the Fe atom affected by protein B is Fe2 and that the ability of this component to alter the coordination modes of Glu243 in H_{red} and H_{ox} may be transmitted through helices E and F. Co-crystal structures of protein B complexed with the hydroxylase in both redox states are needed to investigate these hypotheses and to evaluate the possibility that yet another active site structure might occur in these complexes.

Differences between the frozen and 4 °C structures of H_{ox}

The oxidized hydroxylase structure presented here differs from the previously reported [9] 2.2 Å, 4 °C structure in two respects. First, the bidentate bridging acetate ion has been replaced by a monodentate water bridge and second, the Fe···Fe distance has changed from 3.4 Å to 3.1 Å. We have assigned the monodentate ligand that replaces the acetate bridge as a water molecule because the Fe–O distances are too long for hydroxide coordination. Although to our knowledge there are no (μ-aqua)diiron(III) complexes, there are several hydroxo-bridged diiron(III) compounds in which the average Fe–OH bond length is 1.96 Å [27]. The long 2.5 Å Fe–O distance and presence of the nearby acetate ion in H_{ox} presumably raise the pK_a value of the bridging water molecule.

The substitution of a monoatomic bridge for the acetate bridge was unexpected. The crystal used for the structure determination was grown under exactly the same conditions, which included 50 mM NH_4OAc in the crystallization buffer, as crystals used in the 2.2 Å structure determination. Thus, the crystallization conditions per se probably do not determine the bridge geometry at the active site. An alternative explanation is that the addition of 20 % glycerol as a cryosolvent in the synthetic mother liquor affected the diiron center, even though the crystal was exposed to this solution for less than 1 min. Finally, the loss of the bridging acetate ion could be a consequence of the temperature change. Perhaps one type of coordination is favored at 4 °C whereas a second type of coordination occurs as the temperature is lowered to −160 °C.

Although it is possible that *in vivo* the hydroxylase contains an exogenous carboxylate such as formate in the active site, the new structure offers some insight into the nature of the resting H_{ox} in the absence of acetate-containing buffers. With the assignment of the new monoatomic bridging ligand as a water molecule and the extra electron density in the hydrophobic cavity as a noncoordinated acetate ion, the active site charge remains neutral. The active sites of the ribonucleotide reductase R2 protein in all of its characterized forms are also neutral [21], suggesting that charge neutrality may be a significant feature of these catalytic diiron cores. We propose that, when no acetate has been introduced, the structure of H_{ox} will contain two monoatomic bridges, either one hydroxide ion and one water molecule or two hydroxide ions. The latter would maintain charge neutrality, as would one methoxide and one hydroxide bridge, a likely pair during catalytic turnover. In H_{red}, the active site is also neutral since the acetate ion and hydroxide ion are displaced.

The new Fe···Fe distance of 3.1 Å in H_{ox} differs significantly from the 3.4 Å value observed in the 2.2 Å, 4 °C structure. We are confident that this new Fe···Fe distance of 3.1 Å is real and cannot be attributed to experimental error. The Fe···Fe distances in the two protomers are 3.04 Å and 3.14 Å, averaging to ~3.1 Å, and this agreement supports the conclusion that the difference between 3.1 Å and 3.4 Å is greater than experimental error. Furthermore, the shorter Fe···Fe distance is consistent with the occurrence of two monodentate bridges and the resulting four-membered $\overline{Fe(OH)Fe(OH_2)}$ ring. The present structure determination is not the first indication of such a short Fe···Fe distance in H_{ox}. The Fe···Fe distance obtained from an analysis of EXAFS spectroscopic data for the *M. capsulatus* (Bath) hydroxylase was very dependent on the specific model compounds used to determine fitting parameters [11]. Two Fe···Fe distances of 3.0 Å and 3.4 Å were obtained for samples of the oxidized and mixed valent hydroxylase depending on the choice of these parameters. A short Fe···Fe distance of 3.05 Å was also obtained from an analysis of EXAFS data on the oxidized sMMO hydroxylase from *Methylobacterium* CRL-26 [28].

The EXAFS results raise another issue that must be addressed in analyzing the X-ray structure of the oxidized hydroxylase. In the EXAFS investigations of the *M. capsulatus* (Bath) hydroxylase, many of the oxidized hydroxylase samples were photoreduced to the mixed valent, Fe(II)Fe(III) state in the synchrotron-generated X-ray beam [11,29]. Since the X-ray diffraction data were also collected with synchrotron radiation, it is possible that photoreduction of the diiron center might have occcured in crystals of H_{ox}. We believe that the iron centers in the crystals of H_{ox} used for data collection remained oxidized for two reasons. No trend in Fe–O or Fe–N distances is apparent that would differentiate Fe(II) and Fe(III). In addition, a preliminary single-crystal EXAFS control experiment revealed no shift in the Fe K-edge, indicating that no photoreduction occurred (H. Bufford, A.C.R., B. Hedman, S.J.L. & K.O. Hodgson, unpublished results).

Mechanistic implications

The details of the present two new structure determinations of the diiron center in the sMMO hydroxylase help to sharpen our understanding of the reaction cycle postulated [1,3,8] for the hydroxylation mechanism. In the first step of this cycle, H_{ox} is converted by the reductase and in the presence of protein B to H_{red}. In the next step, H_{red} reacts with dioxygen to form a diiron(III) peroxo intermediate ([7] and K.E. Liu *et al.*, unpublished data). The crystal structure suggests where the Fe–O

bonds in this peroxo species may form, namely, at the positions trans to the N atoms, as indicated in Fig. 6c. In the third step, H_{peroxo} is converted to an intermediate designated Q, which reacts with substrate to form product. The same sites where iron(III)-peroxide bonds in H_{peroxo} may form also demarcate a likely position for the oxidized product alcohol to coordinate before protonation and release from the catalytic center. The structure of H_{ox} supports this hypothesis, since the site in H_{red} occupied only by the water molecule coordinated to Fe1 corresponds to the position of the acetate bridge in the 2.2 Å, 4 °C structure as well as the water bridge in the frozen crystal structure presented here. Methoxide ion may occupy this site during the catalytic cycle. The fact that the dinuclear iron center can breathe, the Fe···Fe distance changing by ~0.3 Å depending on the nature of exogenous ligand bridge, is also consistent with the suggestion that a bridging peroxide might occupy this site in H_{peroxo}.

The presence of electron density, tentatively assigned as a non-coordinated acetate ion in H_{ox} and a noncoordinated water molecule in H_{red}, in the active site cavity provides additional information of possible relevance to the catalytic mechanism. The putative acetate ion and water molecule are located between the labile site on the diiron center and residue Thr213 and form hydrogen bonds to this residue and to a coordinated water molecule in both the oxidized and reduced structures (Figs. 1 and 3). The positioning of these species in the active site cavity indicates how protons might be shuttled to the diiron center during the reaction cycle. The threonine residue has been compared [9] to a conserved threonine residue in cytochrome $P450_{CAM}$, which has been suggested by site-directed mutagenesis experiments [30] and molecular dynamics simulations [31] to supply protons in the formation of intermediates and products during the catalytic cycle. When Thr252 is mutated to a non-hydrogen bonding residue, the reaction is uncoupled, affording hydrogen peroxide and water rather than product alcohol. Since Thr213 is hydrogen bonded through an acetate ion (H_{ox}) or a water molecule (H_{red}) to the postulated site of chemical reactivity, it too may function as a proton donor in the hydroxylation mechanism. Alternatively, Thr213 may be involved not only in proton transfer, but also in triggering changes in the active site caused by the binding of protein B. Since Thr213 is housed on the E helix which is located in the proposed binding domain for protein B [9], this component may affect the diiron center by perturbing the hydrogen bonding network involving Thr213.

Thr213 is one of only two protonated amino acid residues in the active site cavity, the other being Cys151. The sulfhydryl atom of Cys151 is located 7 Å from Fe1, and occupies the same position that the functionally important tyrosyl radical does in the R2 protein. The remainder of residues in the active site cavity are hydrophobic, comprising Ile217, Ile239, Phe236, Leu110, Phe188, Ala117, Phe192, Leu204, and Gly208. In H_{ox}, these residues form a pocket around the acetate ion, as shown in Figure 7, keeping it proximal to the diiron center. In particular, residues Phe188 and Phe192 serve to 'clamp' the acetate ion into the active site, and may play a similar role in facilitating CH_4 and O_2 binding. The hydroxylase oxidizes a wide variety of hydrocarbon substrates [32,33], and these phenylalanine residues may undergo conformational changes in order to accommodate substrates of varying shapes and sizes.

In conclusion, the structures reported here should help us to understand the mechanism of hydroxylation by the sMMO hydroxylase. In the diiron(II) center, residue Glu243 undergoes a carboxylate shift, resulting in a new coordination mode not previously observed in biological diiron centers. The flexibility of this carboxylate ligand seems to be important both for the formation of the diiron(II) center and probably for species active in the catalytic cycle. The structure of the diiron(II) center further reveals open coordination sites and sites containing readily displaced water molecules, which are available to bind dioxygen in the formation of the peroxo intermediate. The diiron(III) center in the frozen crystal has undergone a significant rearrangement from what was previously observed at 4 °C, delineating likely sites of intermediate and product binding as well as the flexibility of the center. This flexibility, which depends on the type of exogenous ligand bridge, may be an important feature for the coordination changes that must occur during the reaction cycle. Finally, an acetate ion and a water molecule, located in the active site cavities of H_{ox} and H_{red}, respectively, demonstrate how the substrate can be held in place for oxidation, and delineate a possible proton relay or hydrogen bonding trigger path from Thr213 to the dinuclear iron centers.

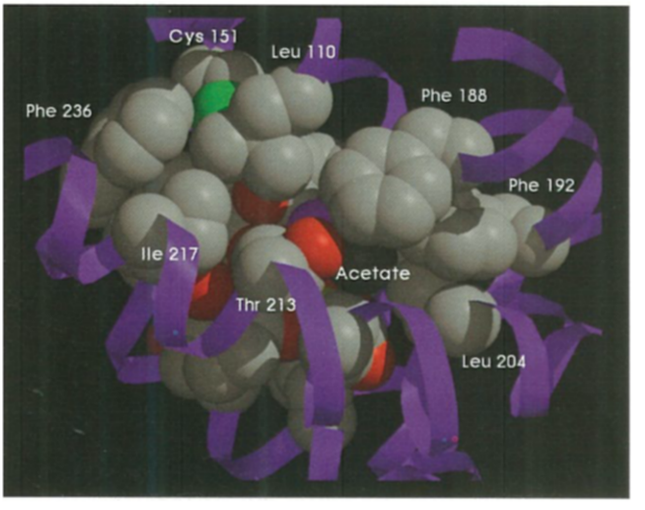

Fig. 7. Space-filling representation of the active site cavity in H_{ox} showing some of the hydrophobic residues as well as Thr213. The acetate ion, shown in magenta (oxygen atom) and gray (carbon atom), interacts with Thr213. Residues Phe188 and Phe192 may anchor the acetate ion and other exogenous ligands in place.

Significance

Methane oxidation by the sMMO system occurs at a catalytic dinuclear iron center in the 251 kDa hydroxylase enzyme. As isolated, the center is in the diiron(III) state (H_{ox}) and is reduced by two electrons during the first step in the catalytic cycle to the diiron(II) state (H_{red}). This fully reduced species then reacts with dioxygen to form two intermediates, a diiron(III) peroxo (H_{peroxo}) and a second species, designated Q, of unknown composition. Q reacts with substrate, methane, to form product, methanol. A comprehensive understanding of methane oxidation by sMMO is of importance for several reasons, including the potential use of the chemistry employed by methanotrophic bacteria in the bioremediation of contaminated drinking water and oil spills, and the development of methods to use natural supplies of methane gas more efficiently.

Here we present detailed high resolution structures of the sMMO hydroxylase from *M. capsulatus* (Bath) in its diiron(III) and diiron(II) oxidation states. Data for both structures were collected at −160 °C. In the H_{ox} structure presented here, a bridging acetate ligand seen in the 4 °C structure reported previously [9] is replaced by a monoatomic water bridge, and the Fe···Fe distance decreases from 3.4 Å to 3.1 Å. In the diiron(II) center of H_{red}, one of the iron ligands, Glu243, shifts from the monodentate, terminal binding mode to Fe2 seen in H_{ox} to a mode in which it serves as a bidentate, chelating ligand to Fe2 as well as a monodentate bridging ligand between Fe1 and Fe2. The structures delineate possible sites for Fe–O bond formation in H_{peroxo} and Q, and suggest possible roles for Thr213 in proton transfer in the active site cavity.

Materials and methods

Crystal preparation

Crystals of the hydroxylase were prepared as previously described from solutions containing 25 mM Li_2SO_4, 50 mM NH_4OAc, and 5 % polyethylene glycol 4 000 in 25 mM 3-[N-morpholino]propanesulfonic acid (MOPS) buffer, pH 7.0 [34]. Prior to flash-freezing, crystals were transferred briefly to a synthetic solution with the same composition as the crystallization mother liquor, but with a higher polyethylene glycol concentration of 20 %. In addition, 20 % glycerol was added to the solution as a cryosolvent. Crystals were mounted on loops prepared from synthetic fibers and flash frozen at −160 °C by using a Precision Cryogenic Systems, Inc. cryocooling system. Crystals to be reduced to the diiron(II) oxidation state were transferred to a degassed synthetic mother liquor containing 20 % glycerol and equilibrated in an argon filled glove box for ~1 h. Chemical reduction was carried out in the glove box by the addition of 6 mM sodium dithionite and 5 mM methyl viologen, followed by a 75 min incubation. Crystals were then mounted on loops directly from the reducing solution and flash-frozen as described above. Frozen crystals were preserved in liquid nitrogen and transported to the Photon Factory in Tsukuba, Japan and to Stanford Synchrotron Radiation Laboratory (SSRL), Palo Alto, CA for data collection.

Data collection and refinement

At the Photon Factory, a frozen native crystal was mounted, and a high resolution data set was collected by using a modified Weissenberg camera with imaging plates and an Oxford cryocooling system. The R_{sym} for the data set is 0.039 to 1.7 Å resolution, and the data are 77 % complete at 1.7 Å resolution. Upon freezing, the unit cell dimensions contracted from the 4 °C values of 62.6 x 110.1 x 333.5 Å [34] to 61.7 x 109.6 x 330.2 Å. The structure was refined by using X-PLOR [35] with the 2.2 Å, 4 °C structure [9] as a starting model, and the program O [36] was used for all model building. The final R-value is 0.183 to 1.7 Å resolution, and the model contains the same amino acid residues as the 2.2 Å resolution model in addition to 1487 water molecules. The root-mean square (rms) deviations from ideal geometry are 0.010 Å for bond distances and 1.51° for bond angles, and > 99 % of the amino acid residues fall within allowed regions of a Ramachandran plot [37]. The average error of the atomic coordinates in the refined model was estimated by a Luzzati plot [38] to be ~0.20 Å. Details of the overall structure at 1.7 Å resolution will be presented elsewhere.

A high resolution data set was collected on a frozen reduced crystal at SSRL beamline 7-1 by using a Mar research imaging plate detector (diameter 300 mm) equipped with a 2theta vertical lift and a modified Siemens LT1 cryocooling system. The R_{sym} for the data set is 0.070 to 1.7 Å resolution. The data are 85 % complete to 2.3 Å, and 30 % complete between 2.3 and 1.7 Å. The lack of completeness at higher resolution is not due to weaker diffraction (the R_{sym} in the 1.7 Å resolution shell is 0.086), but to an imperfect data collection strategy with the 2theta lift. The structure was refined by using X-PLOR [35] with the 1.7 Å frozen native structure as a starting model. The final R-value is 0.198 to 1.7 Å resolution, with the inclusion of 986 water molecules, and the rms deviations are 0.012 Å from ideal bond distances and 1.57° from ideal bond angles, with > 99 % of the amino acid residues falling within allowed regions of a Ramachandran plot. According to a Luzzati plot, the error in the refined coordinates is ~0.25 Å.

Acknowledgements: This work was supported by grants from the National Institute of General Medical Sciences (GM32134 to S.J.L. and GM48388 to C.A.F. and S.J.L.) and from the Claudia Adams Barr Foundation (C.A.F.). A.C.R. is the recipient of NIGMS postdoctoral fellowship GM15914. We thank B.E. Earp and D.A. Whittington for assistance with data collection, the staffs at SSRL and the Photon Factory for support, and P.A. Karplus for helpful discussions.

References

1. Lipscomb, J.D. (1994). Biochemistry of the soluble methane monooxygenase. *Annu. Rev. Microbiol.* **48**, 371–399.
2. Rosenzweig, A.C. & Lippard, S.J. (1994). Determining the structure of a hydroxylase enzyme that catalyzes the conversion of methane to methanol in methanotrophic bacteria. *Accounts Chem. Res.* **27**, 229–236.
3. Liu, K.E. & Lippard, S.J. (1995). Studies of the soluble methane monooxygenase protein system: structure, component interactions, and hydroxylation mechanism. *Adv. Inorg. Chem.*, in press.
4. Lee, S.-K., Nesheim, J.C. & Lipscomb, J.D. (1993). Transient

intermediates of the methane monooxygenase catalytic cycle. *J. Biol. Chem.* **268**, 21569–21577.
5. Lee, S.-K., Fox, B.G., Froland, W.A., Lipscomb, J.D. & Münck, E. (1993). A transient intermediate of the methane monooxygenase catalytic cycle containing an $Fe^{IV}Fe^{IV}$ cluster. *J. Am. Chem. Soc.* **115**, 6450–6451.
6. Liu, K.E., Wang, D., Huynh, B.H., Edmondson, D.E., Salifoglou, A. & Lippard, S. J. (1994). Spectroscopic detection of intermediates in the reaction of dioxygen with the reduced methane monooxygenase hydroxylase from *Methylococcus capsulatus* (Bath). *J. Am. Chem. Soc.* **116**, 7465–7466.
7. Liu, K.E., *et al.*, & Lippard, S.J. (1995). Characterizaton of a diiron(III) peroxo intermediate in the reaction cycle of methane monooxygenase hydroxylase from *Methylococcus capsulatus* (Bath). *J. Am. Chem. Soc.* **117**, 4987–4990.
8. Feig, A.L. & Lippard, S.J. (1994). Reactions of non-heme iron(II) complexes with dioxygen in chemistry and biology. *Chem. Rev.* **94**, 759–805.
9. Rosenzweig, A.C., Frederick, C.A., Lippard, S.J. & Nordlund, P. (1993). Crystal structure of a bacterial non-haem iron hydroxylase that catalyses the biological oxidation of methane. *Nature* **366**, 537–543.
10. DeRose, V., Liu, K.E., Lippard, S.J. & Hoffman, B. (1993). Proton ENDOR identification of bridging hydroxide ligands in mixed-valent diiron centers of proteins: methane monooxygenase and semimet azidohemerythrin. *J. Am. Chem. Soc.* **115**, 6440–6441.
11. DeWitt, J. G., *et al.*, & Lippard, S. J. (1991). X-ray absorption, Mössbauer, and EPR studies of the dinuclear iron center in the hydroxylase component of methane monooxygenase. *J. Am. Chem. Soc.* **113**, 9219–9235.
12. Herold, S., Pence, L.E. & Lippard, S.J. (1995). Carboxylate-bridged diiron(II) complexes, including a new model for the reduced methane monooxygenase hydroxylase and the R2 protein of ribonucleotide reductase. *J. Am. Chem. Soc.* **117**, in press.
13. Pulver, S., Froland, W.A., Fox, B.G., Lipscomb, J.D. & Solomon, E.I. (1993). Spectroscopic studies of the coupled binuclear non-heme iron active site in the fully reduced hydroxylase component of methane monooxygenase: comparison to deoxy and deoxy-azide hemerythrin. *J. Am. Chem. Soc.* **115**, 12409–12422.
14. Goldberg, D.P., Telser, J., Bastos, C.M. & Lippard, S.J. (1995). Five structurally analogous carboxylate-bridged trinuclear ferrous complexes. *Inorg. Chem* **34**, 3011–3024.
15. Rardin, R.L., Tolman, W.B. & Lippard, S.J. (1991). Monodentate carboxylate complexes and the carboxylate shift: implications for polymetalloprotein structure and function. *New. J. Chem.* **15**, 417–430.
16. Tolman, W.B., Liu, S., Bentsen, J.G. & Lippard, S.J. (1991). Models of the reduced forms of polyiron-oxo proteins: an asymmetric, triply carboxylate bridged diiron(II) complex and its reaction with dioxygen. *J. Am. Chem. Soc.* **113**, 152–164.
17. Hardman, K.D., Agarwal, R.C. & Freiser, M.J. (1982). Manganese and calcium binding sites of concanavalin A. *J. Mol. Biol.* **157**, 69–86.
18. Fontecave, M., Nordlund, P., Eklund, H. & Reichard, P. (1992). The redox centers of ribonucleotide reductase of *Escherichia coli*. *Adv. Enzym.* **65**, 147–153.
19. Stubbe, J. (1990). Ribonucleotide reductases: amazing and confusing. *J. Biol. Chem.* **265**, 5329–5332.
20. Nordlund, P., Sjöberg, B.-M. & Eklund, H. (1990). Three dimensional structure of the free radical protein of ribonucleotide reductase. *Nature* **345**, 593–598.
21. Åberg, A. (1993). Ribonucleotide reductase from *Escherichia coli*: structural aspects of protein function. Ph.D. thesis, Stockholm University.
22. Nordlund, P. & Eklund, H. (1993). Structure and function of the *Escherichia coli* ribonucleotide reductase protein R2. *J. Mol. Biol.* **232**, 123–164.
23. Liu, K. E. & Lippard, S. J. (1991). Redox properties of the hydroxylase component of methane monooxygenase from *Methylococcus capsulatus* (Bath). *J. Biol. Chem.* **266**, 12836–12839; 24859.
24. Ortiz de Montellano, P.R. (1986). *Cytochrome P-450: Structure, Mechanism, and Biochemistry.* Plenum Press, New York.
25. Rosenzweig, A.C., Feng, X. & Lippard, S.J. (1991). Studies of methane monooxygenase and alkane oxidation model complexes. In *IUCCP Symposium on Applications of Enzyme Biotechnology.* (Kelly, J.W. & Baldwin, T.O. eds), pp. 69–85, Plenum Press, New York.
26. Fox, B.G., Liu, Y., Dege, J.E. & Lipscomb, J.D. (1991). Complex formation between the protein components of methane monooxygenase from *Methylosinus trichosporium* OB3b. *J. Biol. Chem.* **266**, 540–550.
27. Turowski, P.N., Armstrong, W.H., Liu, S., Brown, S.N. & Lippard, S.J. (1994). Synthesis and characterization of hydroxo-bridged diiron(III) complexes containing carboxylate or phosphate ester bridges: comparisons to diiron(III) proteins. *Inorg. Chem.* **35**, 636–645.
28. Prince, R.C., George, G.N., Savas, J.C., Cramer, S.P. & Patel, R.N. (1988). Spectroscopic properties of the hydroxylase of methane monooxygenase. *Biochim. Biophys. Acta* **952**, 220–229.
29. DeWitt, J.G., Rosenzweig, A.C., Hedman, B., Lippard, S.J. & Hodgson, K.O. (1995). X-ray absorption spectroscopic studies of the diiron center in methane monooxygenase in the presence of substrate and coupling protein of the enzyme system. *Inorg. Chem.* **34**, 2505–2515.
30. Raag, R., Martinis, S.A., Sligar, S.G. & Poulos, T.L. (1991). Crystal structure of the cytochrome $P450_{CAM}$ active site mutant Thr252Ala. *Biochemistry* **30**, 11420–11429.
31. Harris, D.L. & Loew, G.H. (1994). A role for Thr252 in cytochrome $P450_{CAM}$ oxygen activation. *J. Am. Chem. Soc.***116**, 11671–11674.
32. Colby, J., Stirling, D.I. & Dalton, H. (1977). The soluble methane monooxygenase of *Methylococcus capsulatus* (Bath). *Biochem. J.* **165**, 395–402.
33. Liu, K.E., Johnson, C.C., Newcomb, M. & Lippard, S.J. (1993). Radical clock studies and kinetic isotope effect studies of the hydroxylation of hydrocarbons by methane monooxygenase. *J. Am. Chem. Soc.* **115**, 939–947.
34. Rosenzweig, A.C., Frederick, C.A. & Lippard, S.J. (1992). Crystallization and preliminary X-ray analysis of the methane monooxygenase hydroxylase protein from *Methylococcus capsulatus* (Bath). *J. Mol. Biol.* **227**, 283–285.
35. Brünger, T.A., Kuriyan, J. & Karplus, M. (1987). Crystallographic R-factor refinement by molecular dynamics. *Science* **235**, 458–460.
36. Jones, T.A., Bergdoll, M. & Kjeldgaard, M. (1989). In *Crystallographic Computing and Modeling Methods in Molecular Design.* (Bugg, C. & Ealick, S. eds), Springer-Verlag, New York,
37. Ramachandran, G.N. & Sassiekharan, V. (1968). Conformation of polypeptides and proteins. *Adv. Protein Chem.* **28**, 283–437.
38. Luzatti, P.V. (1952). Traitement statistique des erreurs dans la determination des structures cristallines. *Acta Crystallogr.* **5**, 802–810.

Received: **24 May 1995**; revisions requested: **31 May 1995**; revisions received: **5 June 1995**. Accepted: **5 June 1995**.